

pubs.acs.org/JACS Communication

Metal—Organic Layers with Photosensitizer and Pyridine Pairs Activate Alkyl Halides for Photocatalytic Heck-Type Coupling with Olefins

Yingjie Fan, Abigail L. Blenko, Steven Labalme, and Wenbin Lin*



Cite This: J. Am. Chem. Soc. 2024, 146, 7936-7941



ACCESS I

Metrics & More

Article Recommendations

Supporting Information

ABSTRACT: Photochemical generation of alkyl radicals from haloalkanes often requires strong energy input from ultraviolet light or a strong photoreductant. Haloalkanes can alternatively be activated with nitrogen-based nucleophiles through a sequential $S_{\rm N}2$ reaction and single-electron reduction to access alkyl radicals, but these two reaction steps have opposite steric requirements on the nucleophiles. Herein, we report the design of Hf_{12} metal—organic layers (MOLs) with iridium-based photosensitizer bridging ligands and secondary-building-unit-supported pyridines for photocatalytic alkyl radical generation from haloalkanes. By bringing the photosensitizer and pyridine pairs in proximity, the MOL catalysts allowed facile access to the pyridinium salts from $S_{\rm N}2$ reactions between haloalkanes and pyridines and at the same time enhanced electron transfer from excited photosensitizers to pyridinium salts to facilitate alkyl radical generation. Consequentially, the MOLs efficiently catalyzed Heck-type cross-coupling reactions between haloalkanes and olefinic substrates to generate functionalized alkenes. The MOLs showed 4.6 times higher catalytic efficiency than the homogeneous counterparts and were recycled and reused without a loss of catalytic activity.

adical chemistry involving single-electron processes has been widely explored in the recent renaissance of photoand electro-catalysis for chemical synthesis. 1,2 However, radical generation from most substrates requires strong energy input from ultraviolet light or a powerful photoreductant, which compromises reaction selectivity.3 These substrates can be prefunctionalized to enhance their photoredox activity. For example, carboxylic acids can be converted to redox-active esters which react with photoreductants to form decarboxylated radicals.⁴ Aldehydes can be converted to α -acetoxy iodides which are easier to reduce than the aldehydes. Haloalkanes can be activated via a halogen atom transfer process, wherein heteroatom-based radicals are generated (from silanes, amines, etc.) and used for halogen atom abstraction and alkyl radical generation,^{6,7} or an S_N2-based strategy, wherein alkyl dithiocarbamates are converted to alkyl radicals via photoinduced C-S bond cleavage (Figure 1a).8

Nitrogen-based nucleophiles have shown potential in S_N2 -based activation of haloalkanes. In particular, Katritzky (pyridinium) salts, originally accessed from primary amines and 2,4,6-triphenylpyrylium tetrafluoroborate, have served as radical precursors in deaminative Suzuki–Miyaura and Hecktype coupling reactions (Figure 1b). 11–14 The reactivity of pyridinium salts is highly sensitive to their steric properties. 15–18 Pyridinium salts with large *ortho* substituents are readily reduced to generate radicals, but difficult to access via S_N2 reactions between pyridines and haloalkanes. The opposite steric requirements for pyridinium salts limit the use of pyridines as nucleophiles in photocatalytic activation of haloalkanes. We hypothesized that a photosensitizer (PS) and pyridine pairs can be installed on metal—organic layers

(MOLs) to facilitate photocatalytic alkyl radical generation from haloalkanes.

As a two-dimensional version of metal-organic frameworks (MOFs), 19-23 MOLs not only inherit the tunable nature and crystalline structures of MOFs²⁴⁻³² but also possess freely accessible and modifiable active sites to enable efficient catalysis.33-41 We have demonstrated hierarchical modifications of MOLs for photocatalytic reactions by bringing PSs and catalytic sites in proximity to improve reaction kinetics. 42,43 We recently designed biomimetic MOL catalysts comprising heme, amino acids, and PSs for artificial photosynthesis (Figure 1c).⁴⁴ These precedents prompted us to design PS and pyridine pairs on MOLs for the cooperative photochemical alkyl radical generation from haloalkanes (Figure 1d). We hypothesized that the proximity of PSs and pyridines could promote electron transfer to and radical dissociation from unsubstituted pyridinium salts, which could be readily accessed via S_N2 reactions of pyridines and haloalkanes.

Herein, we report the design of Hf_{12} MOLs with iridium-based photosensitizing bridging ligands and secondary building unit (SBU)-supported pyridines for photocatalytic radical generation from haloalkanes. SBU-supported pyridines reacted with haloalkanes to form pyridinium salts, which were reduced by nearby photoexcited Ir-based PSs to generate alkyl radicals for Heck-type coupling with alkenes. The MOL catalyst

Received: January 7, 2024 Revised: March 8, 2024 Accepted: March 11, 2024 Published: March 13, 2024





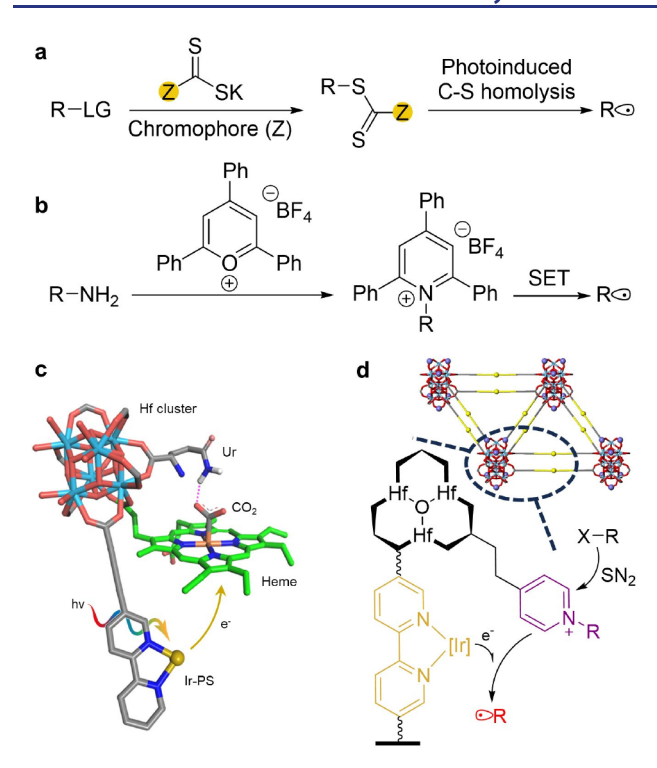


Figure 1. (a) Activation of haloalkanes by dithiocarbamates. (b) Alkyl radical generation from single-electron reduction of pyridinium salts. (c) Biomimetic active sites in MOLs comprising PS, heme, and amino acid cocatalysts for artificial photosynthesis. (d) PS and pyridine pairs on an MOL for the activation of haloalkanes.

showed 4.6 times higher catalytic efficiency than the homogeneous counterpart and was used in 5 consecutive cycles without loss of activities.

The Hf-IrF MOL was synthesized via a solvothermal reaction between HfCl₄ and IrF {Ir(DBB)[dF(CF₃)ppy]⁺, DBB = 4.4'-di(4-benzoato)-2.2'-bipyridine, dF(CF₃)ppy = 2-(2,4-difluorophenyl)-5-(trifluoromethyl)pyridine)} in *N,N*-dimethylformamide with trifluoroacetic acid (TFA) modulator at 80 °C (Figure 2a). 45 **Hf-IrF** was modified with 4-pyridinepropionic acid (PPA) via a carboxylate exchange reaction to afford Hf-IrF-PPA. Hf-IrF and Hf-IrF-PPA showed powder X-ray diffraction (PXRD) patterns similar to the simulated one based on the hexagonal structure of Hf-IrF (Figure 2b). Transmission electron microscopy (TEM) imaging revealed nanoplates of Hf-IrF and Hf-IrF-PPA with diameters of 100-300 nm (Figure 2c-d), whereas atomic force microscopy (AFM) gave thicknesses of 1.5 and 2 nm for Hf-IrF and Hf-IrF-PPA, respectively (Figure 2e-f, 2h-i). These thicknesses matched the heights of the Hf₁₂ clusters and PPA-modified Hf₁₂ SBUs, respectively. The ¹H NMR spectrum of digested Hf-IrF-PPA indicated complete replacement of TFA by PPA with a PPA to IrF ratio of 1:1 (Figure 2g), leading to a formula of $Hf_{12}(\mu_3-O)_8(\mu_3-OH)_8(\mu_2-OH)_8$ OH)₆(IrF)₆(PPA)₆. The IR spectrum of Hf-IrF-PPA supported the presence of PPA with a peak at 1707 cm⁻¹ (Figures 3c, S13).

We tested cross-coupling of ethyl bromoacetate (1a), an activated haloalkane, with 1,1-diphenylethylene (2a) using IrF and substituted pyridines as catalysts (Tables S1, S2). Pyridine, DMAP, and 4-phenylpyridine produced ethyl 4,4-diphenylbut-3-enoate (3a) in low yields. With 120 mol % 2,4,6-collidine, the reaction proceeded smoothly in acetonitrile at 50 °C under

440 nm irradiation to give **3a** in 84% yield. Thus, *ortho* substituents are essential for pyridinium reduction and alkyl radical generation. However, sterically hindered ethyl 2-bromo propionate (**1c**) and unactivated 1-bromo-3-phenyl-propane (**1j**) reacted with **2a** to afford **3j** and **3q** in 49%, and 0%, respectively (see Supporting Information S6 for details).

Hf-IrF-PPA catalyzed photocatalytic coupling of 1a and 2a to afford 3a in 82% yield in the presence of stochiometric amounts of 1,8-bis(dimethylamino)naphthalene (proton sponge) and NaI. The proton sponge served as a base to neutralize the acid generated from the cross-coupling whereas NaI likely transformed 1a into ethyl iodoacetate to enhance the S_N2 reaction between 1a and PPA. Interestingly, although 4-phenylpyridine and 2,4,6-collidine outperformed pyridine in homogeneous reactions, they were outperformed by PAA in MOL-catalyzed reactions (Table S3). This result suggests enhanced alkyl radical generation from pyridinium salts on the MOL due to the proximity between the IrF and PPA pair.

We next investigated the substrate scope of Heck-type coupling reactions. As shown in Table 1, 1a reacted with silyl enol ethers 2b, 2c, and 2d to give 3b, 3c, and 3d in >90% yields. Styrene derivatives 2e, 2f, and 2g also coupled with 1a to afford 3e, 3f, and 3g as E isomers in 51–62% yields. Indene (2h) reacted with 1a to give 3h in a 55% yield. A reaction between 1a and nonactivated 1-methylcyclohexene produced three isomers of cross-coupling products in 28% total yield (see Supporting Information S6 for details). Electron-donating and aromatic substituents in the olefins were generally favored in the reactions, suggesting a cationic intermediate for double bond formation. Other activated haloalkanes, including 2bromo acetamide (1b) and ethyl 2-bromo propionate (1c), smoothly reacted with 2a to give 3i and 3j in 89% and 78% yields, respectively. Substituted benzyl bromides 1d, 1e, and 1f reacted with 2a to afford 3k, 3l, and 3m in approximately 80% yields. Alkyl chlorides, including benzyl chloride (1g) and 2chloro acetonitrile (1h), also reacted with 2a to afford 3n and 30 in 68% and 84% yields, respectively.

Hf-IrF-PPA did not catalyze cross-coupling reactions between nonactivated primary alkyl bromides and 2a, likely due to the limited reduction potential of IrF. We synthesized a new MOL, Hf-Ir($C \land N$)₃, with a more reducing photosensitizing ligand, $Ir(C \land N)_3$ {with one 4 4'-(5-(4-carboxyphenyl)pyridin-2-yl)-[1,1'-biphenyl]-4-carboxylate and two 2-phenylpyridine ligands. Indeed, the excited state of $Ir(C \land N)_3$ was more reducing than that of IrF (Figure S20). Hf-Ir($\mathbb{C} \land \mathbb{N}$)₃ showed an ultrathin nanoplate morphology with 3-4 layers of Hf₁₂ hexagonal networks and was modified with PPA to afford Hf-Ir($C \land N$)₃-PPA (see S2.3 for details, Figures S8–S11). Hf- $Ir(C \land N)_3$ -PPA successfully catalyzed cross-coupling of 4bromo-1-butene (1i), 1j, and 3-bromophenoxypropane (1k) with 2a to give 3p, 3q, and 3r in 55%, 52% and 62% yields, respectively. Under identical conditions, the homogeneous catalyst produced 3p, 3q, and 3r in 10%, 7%, and 17% yields, respectively.

Hf-IrF-PPA catalyzed the cross-coupling between 4-hydroxylcoumarin and 1-bromo-1-phenylpropane to produce Phenprocoumon, a blood-thinner medicine, in 71% yield (Table 1). Hf-IrF-PPA was recycled by centrifugation and used in five cycles of cross-coupling between 1a and 2a without a loss of catalytic activity (Figure 3e). The recovered Hf-IrF-PPA remained crystalline (Figure S14). In the sixth cycle, Hf-IrF-PPA was removed by centrifugation, and the yield of 3a

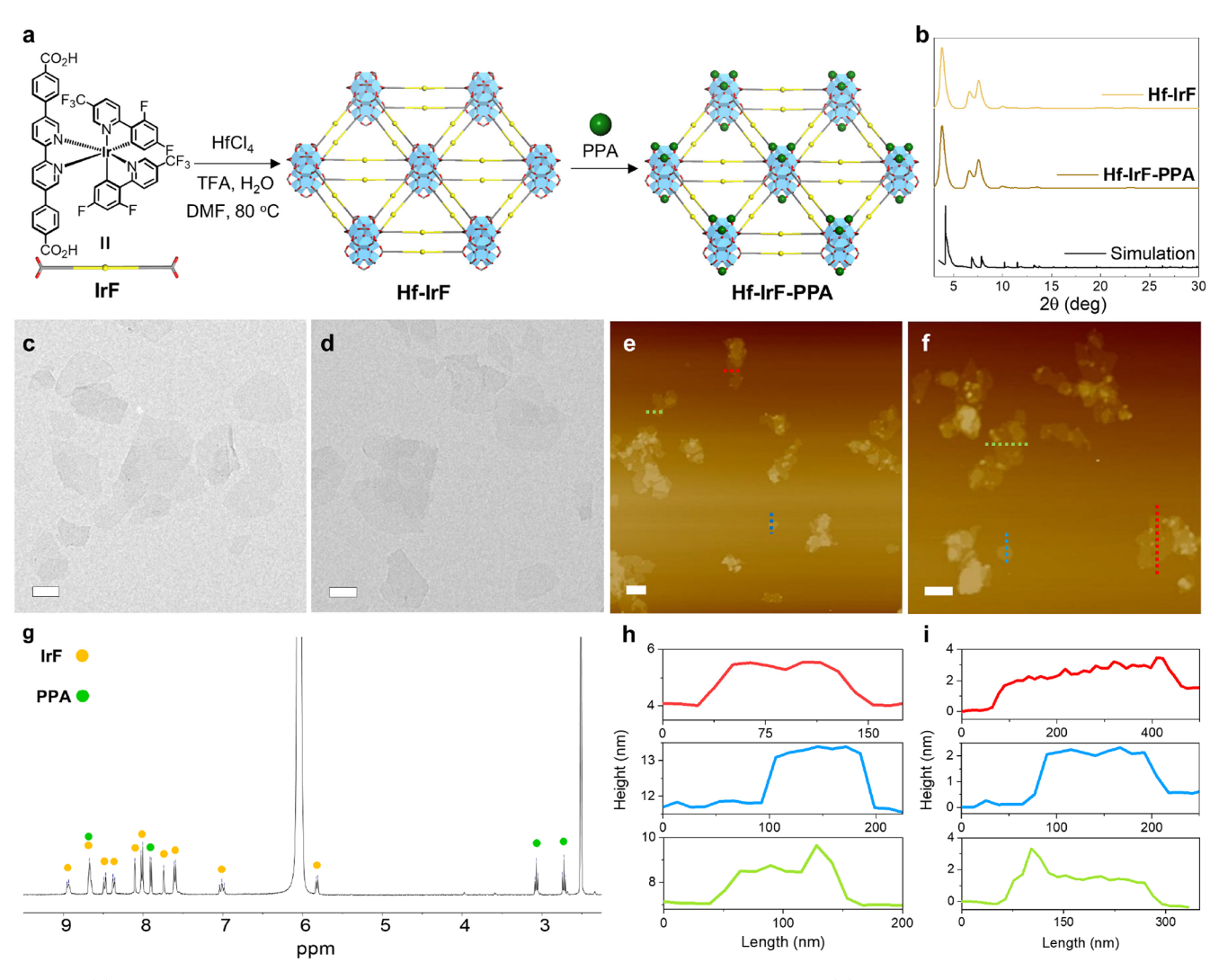


Figure 2. (a) Synthetic scheme for **Hf-IrF-PPA**. Gray, C; blue, Hf; red, O; yellow, **IrF**; green, PPA. (b) PXRD patterns of **Hf-IrF** and **Hf-IrF-PPA** along with the simulated one for **Hf-IrF**. (c-f) TEM and AFM images of **Hf-IrF** and **Hf-IrF-PPA**. (Scale bar: 200 nm) (g) ¹H NMR spectrum of digested **Hf-IrF-PPA**. (h—i) Height profiles of **Hf-IrF** and **Hf-IrF-PPA**. The colored height profiles in h and i correspond to the colored dashed lines in e and f, respectively.

dropped to 3% with <1% Hf leaching into the solution. This experiment demonstrated the heterogeneity of MOL-catalyzed reactions.

We performed several control experiments to gain insights into the MOL catalysts (Figure 3a). A mixture of 1 mol % IrF and 1 mol % pyridine catalyzed the coupling between 1a and 2a to give 3a in 18% yield. Thus, the MOL catalyst outperformed the homogeneous control by 4.6-fold. IrF alone or pyridine alone afforded 3a in 10% and 0%, respectively. Without LED irradiation, Hf-IrF-PPA did not catalyze the reaction. The addition of 2,2,6,6-tetramethyl-1-piperidinyloxy (TEMPO) to the Hf-IrF-PPA-catalyzed reaction decreased the yield of 3a from 82% to 11%. A reaction at room temperature afforded 3a in 68% yield. These results indicate a strong synergy between IrF and PPA on MOL and the radical nature of the cross-coupling reaction.

Hf-IrF competently catalyzed the reaction of 1-(2-ethoxy-2-oxoethyl)pyridinium (4) and 2a to afford 3a in 63% yield (Figure 3b), suggesting 4 as a reaction intermediate in the cross-coupling between 1a and 2a. An electron donor–acceptor complex between the pyridinium salt and NaI or proton sponge was observed under the catalytic condition, 47,48

but did not catalyze the cross-coupling reaction (Figure S19). After treatment of 1 mol % of Hf-IrF-PPA with 1a in acetone at 50 °C for 18 h, the recovered MOL showed a carbonyl peak at 1731 cm⁻¹ (Figure 3c) which matched that of the alkylated PPA, 4-(2-carboxyethyl)-N-(ethoxycarbonylmethyl)pyridinium bromide (PPA+). Hf-Ir-PPA+ also showed a shift of the C=N stretching peak to 1642 cm⁻¹ from 1615 cm⁻¹ for Hf-IrF-PPA. The ¹H NMR spectrum of the digested MOL gave a PPA⁺ to IrF ratio of 1:1, indicating complete conversion of PPA to PPA⁺ (Figure S16). Importantly, photoluminescence quenching of Hf-Ir-PPA+ was highly dependent on PPA+ loadings (Figure 3d). Hf-Ir-PPA+ showed 10.8 times faster quenching of IrF by PPA+ than the homogeneous control, which indicates faster electron transfer from the photoexcited Hf-Ir to the PPA+ on the MOL and the superiority of the MOL catalyst over the homogeneous control.

Based on these results, we propose a reaction mechanism for Hf-IrF-PPA-catalyzed Heck-type coupling reactions in Figure 3f. The installation of IrF and PPA on the MOL creates the catalyst pair in proximity (with a separation of ~ 11 Å, Figure S21). At elevated temperatures, the pyridine undergoes an S_N2 reaction with haloalkane to form a pyridinium salt, which is

entry	variation catalyst	yield of 3a(%)
1	Hf-IrF-PPA (1 mol%)	82
2	IrF-PS (1 mol%) + pyridine (1 mol9	%) 19
3	IrF-PS (1 mol%)	10
4_	Pyridine (1 mol%)	0
4 5 ^a	Hf-IrF-PPA (1 mol%)	0
6 ^b	Hf-IrF-PPA (1 mol%)	11
7 ∘	Hf-IrF-PPA (1 mol%)	68
8	Hf-IrF-Ph (1 mol%)	5

- ^a Reaction was run in the dark. ^b 1 eqv TEMPO was added.
- ^c Reaction was run under room temperature.

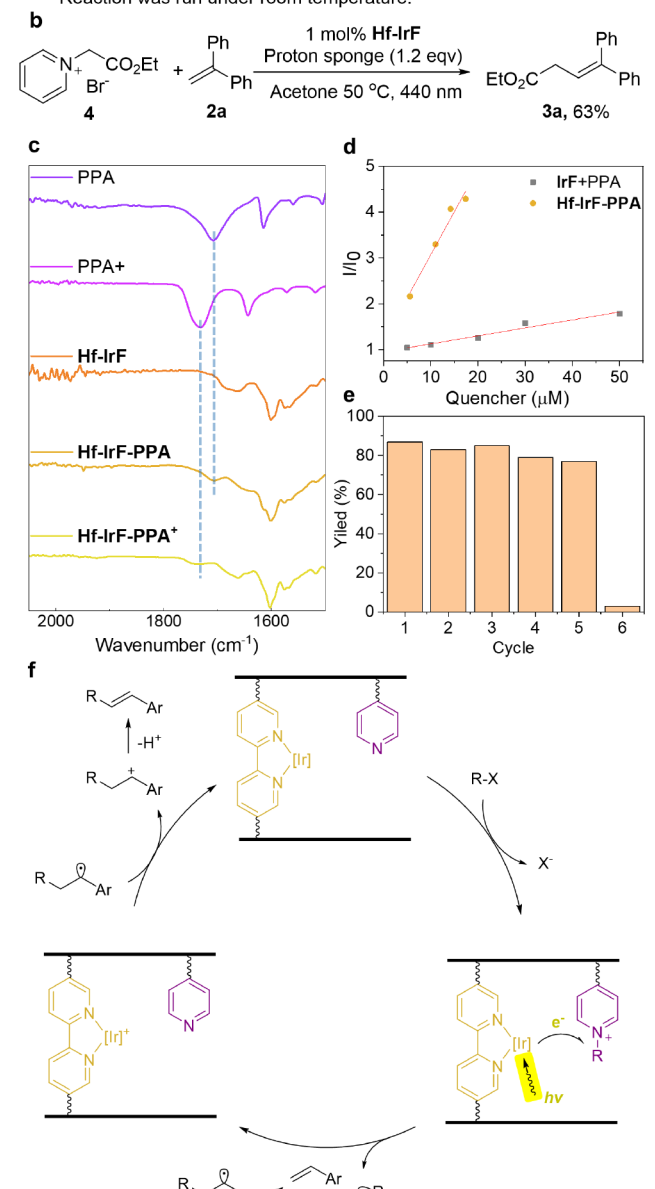


Figure 3. (a) Control experiments. (b) Hf-IrF-catalyzed crosscoupling between 4 and 2a. (c) IR spectra of PPA, PPA+, Hf-IrF, Hf-IrF-PPA, and Hf-IrF-PPA⁺. (d) Photoluminescence quenching of IrF by PPA+ in homogeneous solutions and in Hf-IrF-PPA+. (e) Yield of 3a in 5 consecutive reactions between 1a and 2a. (f) Proposed mechanism for Hf-IrF-PPA-catalyzed Heck-type coupling reactions.

Table 1. Substrate Scope for MOL-Catalyzed Heck-Type Radical Coupling Reactions

^aReactions were performed with 0.2 mmol of 1, 0.3 mmol of 2, 0.2 mmol of NaI, 0.24 mmol of proton sponge, and 1 mol % Hf-IrF-PPA in 4 mL of acetone at 50 °C under LED irradiation (440 nm) for 18 h. ^bReactions were performed with Hf-Ir($\mathbb{C} \wedge \mathbb{N}$)₃-PPA.

promptly reduced by adjacent IrF under light irradiation to generate an alkyl radical. The acceleration of this step by the proximity between PSs and pyridines allows the use of more nucleophilic pyridines without 2,6-substituents. The alkyl radical then adds to an olefin quickly. The adduct is oxidized by [IrF]+ to generate a carbocation intermediate which undergoes E1-type elimination to afford the cross-coupled product. 49,50 This mechanism explains a decrease in the reaction yield with sterically hindered or nonactivated

haloalkanes due to the slower pyridinium formation via the $S_{\rm N}2$ reaction. Furthermore, electron-poor olefin acceptors did not work in the reactions due to the formation of a high-energy carbocation intermediate.

In summary, we designed MOL catalysts with photosensitizer and pyridine pairs for Heck-type cross-coupling reactions between haloalkanes and olefins. The proximity of photosensitizers and pyridines on the MOL allows facile access to the pyridinium salts from $S_{\rm N}2$ reactions between haloalkanes and pyridines and enhances electron transfer from excited PSs to non-ortho-substituted pyridinium salts to facilitate alkyl radical generation. As a result, the MOLs efficiently catalyze Heck-type cross-coupling reactions between haloalkanes and olefinic substrates to generate functionalized alkenes. The MOL catalyst shows 4.6 times higher catalytic efficiency than the homogeneous counterpart and is used in 5 consecutive cycles without loss of catalytic activities. This work establishes MOLs as a unique molecular material platform to discover new photoredox catalysts for challenging organic transformations.

ASSOCIATED CONTENT

Supporting Information

The Supporting Information is available free of charge at https://pubs.acs.org/doi/10.1021/jacs.4c00258.

Materials and methods, synthesis and characterization of MOLs, general procedure for reaction optimization, catalytic reactions and product characterization, control experiments, mechanistic studies, examples of unreactive substrates, NMR spectra of all compounds. (PDF)

AUTHOR INFORMATION

Corresponding Author

Wenbin Lin — Department of Chemistry, The University of Chicago, Chicago, Illinois 60637, United States; orcid.org/0000-0001-7035-7759; Email: wenbinlin@uchicago.edu

Authors

Yingjie Fan — Department of Chemistry, The University of Chicago, Chicago, Illinois 60637, United States;
orcid.org/0000-0003-1857-5788

Abigail L. Blenko – Department of Chemistry, The University of Chicago, Chicago, Illinois 60637, United States

Steven Labalme – Department of Chemistry, The University

of Chicago, Chicago, Illinois 60637, United States

Complete contact information is available at: https://pubs.acs.org/10.1021/jacs.4c00258

Notes

The authors declare no competing financial interest.

ACKNOWLEDGMENTS

We acknowledge the National Science Foundation (CHE-2102554) and the University of Chicago for funding support and the MRSEC Shared User Facilities at the University of Chicago (DMR-1420709) for instrument access.

REFERENCES

(1) Yan, M.; Kawamata, Y.; Baran, P. S. Synthetic Organic Electrochemical Methods Since 2000: On the Verge of a Renaissance. *Chem. Rev.* **2017**, *117* (21), 13230–13319.

- (2) Shaw, M. H.; Twilton, J.; MacMillan, D. W. C. Photoredox Catalysis in Organic Chemistry. J. Org. Chem. 2016, 81 (16), 6898–6926
- (3) Studer, A.; Curran, D. P. Catalysis of Radical Reactions: A Radical Chemistry Perspective. *Angew. Chem., Int. Ed.* **2016**, *55* (1), 58–102.
- (4) Okada, K.; Okamoto, K.; Morita, N.; Okubo, K.; Oda, M. Photosensitized decarboxylative Michael addition through N-(acyloxy)phthalimides via an electron-transfer mechanism. *J. Am. Chem. Soc.* **1991**, *113* (24), 9401–9402.
- (5) Wang, L.; Lear, J. M.; Rafferty, S. M.; Fosu, S. C.; Nagib, D. A. Ketyl radical reactivity via atom transfer catalysis. *Science* **2018**, *362* (6411), 225–229.
- (6) Juliá, F.; Constantin, T.; Leonori, D. Applications of Halogen-Atom Transfer (XAT) for the Generation of Carbon Radicals in Synthetic Photochemistry and Photocatalysis. *Chem. Rev.* **2022**, 122 (2), 2292–2352.
- (7) Zhang, P.; Le, C. C.; MacMillan, D. W. C. Silyl Radical Activation of Alkyl Halides in Metallaphotoredox Catalysis: A Unique Pathway for Cross-Electrophile Coupling. *J. Am. Chem. Soc.* **2016**, *138* (26), 8084–8087.
- (8) Schweitzer-Chaput, B.; Horwitz, M. A.; de Pedro Beato, E.; Melchiorre, P. Photochemical generation of radicals from alkyl electrophiles using a nucleophilic organic catalyst. *Nat. Chem.* **2019**, *11* (2), 129–135.
- (9) Liu, Q.; Yi, H.; Liu, J.; Yang, Y.; Zhang, X.; Zeng, Z.; Lei, A. Visible-Light Photocatalytic Radical Alkenylation of α -Carbonyl Alkyl Bromides and Benzyl Bromides. *Chem.—Eur. J.* **2013**, *19* (16), 5120–5126.
- (10) Su, Y.; Zhang, L.; Jiao, N. Utilization of Natural Sunlight and Air in the Aerobic Oxidation of Benzyl Halides. *Org. Lett.* **2011**, *13* (9), 2168–2171.
- (11) Basch, C. H.; Liao, J.; Xu, J.; Piane, J. J.; Watson, M. P. Harnessing Alkyl Amines as Electrophiles for Nickel-Catalyzed Cross Couplings via C-N Bond Activation. *J. Am. Chem. Soc.* **2017**, *139* (15), 5313–5316.
- (12) Jiang, X.; Zhang, M.-M.; Xiong, W.; Lu, L.-Q.; Xiao, W.-J. Deaminative (Carbonylative) Alkyl-Heck-type Reactions Enabled by Photocatalytic C–N Bond Activation. *Angew. Chem., Int. Ed.* **2019**, *58* (8), 2402–2406.
- (13) Katritzky, A. R.; Manzo, R. H.; Lloyd, J. M.; Patel, R. C. Mechanism of the Pyrylium/Pyridinium Ring Interconversion. Mild Preparative Conditions for Conversion of Amines into Pyridinium Ions. *Angewandte Chemie International Edition in English* **1980**, 19 (4), 306–306.
- (14) Yang, Z.-K.; Xu, N.-X.; Wang, C.; Uchiyama, M. Photoinduced C(sp3)—N Bond Cleavage Leading to the Stereoselective Syntheses of Alkenes. *Chem.—Eur. J.* **2019**, 25 (21), 5433—5439.
- (15) Tcyrulnikov, S.; Cai, Q.; Twitty, J. C.; Xu, J.; Atifi, A.; Bercher, O. P.; Yap, G. P. A.; Rosenthal, J.; Watson, M. P.; Kozlowski, M. C. Dissection of Alkylpyridinium Structures to Understand Deamination Reactions. *ACS Catal.* **2021**, *11* (14), 8456–8466.
- (16) He, F.-S.; Ye, S.; Wu, J. Recent Advances in Pyridinium Salts as Radical Reservoirs in Organic Synthesis. *ACS Catal.* **2019**, 9 (10), 8943–8960.
- (17) Grimshaw, J.; Moore, S.; Thompson, N.; Trocha-Grimshaw, J. Carbon—nitrogen bond cleavage in π -radicals derived by reduction of N-benzyl- and N-allyl-pyridinium salts. *J. Chem. Soc., Chem. Commun.* **1983**, *14*, 783—784.
- (18) Fortage, J.; Peltier, C.; Perruchot, C.; Takemoto, Y.; Teki, Y.; Bedioui, F.; Marvaud, V.; Dupeyre, G.; Pospísil, L.; Adamo, C.; Hromadová, M.; Ciofini, I.; Lainé, P. P. Single-Step versus Stepwise Two-Electron Reduction of Polyarylpyridiniums: Insights from the Steric Switching of Redox Potential Compression. *J. Am. Chem. Soc.* **2012**, *134* (5), 2691–2705.
- (19) Li, H.; Eddaoudi, M.; O'Keeffe, M.; Yaghi, O. M. Design and synthesis of an exceptionally stable and highly porous metal-organic framework. *Nature* **1999**, *402* (6759), 276–279.

- (20) Furukawa, H.; Cordova, K. E.; O'Keeffe, M.; Yaghi, O. M. The Chemistry and Applications of Metal-Organic Frameworks. *Science* **2013**, *341* (6149), No. 1230444.
- (21) Han, X.; Zhang, W.; Chen, Z.; Liu, Y.; Cui, Y. The future of metal—organic frameworks and covalent organic frameworks: rational synthesis and customized applications. *Mater. Horiz.* **2023**, *10* (12), 5337–5342.
- (22) Yin, H.-Q.; Zhang, Z.-M.; Lu, T.-B. Ordered Integration and Heterogenization of Catalysts and Photosensitizers in Metal-/Covalent-Organic Frameworks for Boosting CO₂ Photoreduction. *Acc. Chem. Res.* **2023**, *56* (19), 2676–2687.
- (23) Luo, D.; Wang, X.-Z.; Yang, C.; Zhou, X.-P.; Li, D. Self-Assembly of Chiral Metal—Organic Tetartoid. *J. Am. Chem. Soc.* **2018**, 140 (1), 118–121.
- (24) Cheng, S.; Ouyang, J.; Li, M.; Diao, Y.; Yao, J.; Li, F.; Lee, Y.-F.; Sung, H. H.-Y.; Williams, I.; Xu, Z.; Quan, Y. Charge Separation in Metal-Organic Framework Enables Heterogeneous Thiol Catalysis. *Angew. Chem., Int. Ed.* **2023**, *62* (25), No. e202300993.
- (25) Lin, J.; Ouyang, J.; Liu, T.; Li, F.; Sung, H. H.-Y.; Williams, I.; Quan, Y. Metal-organic framework boosts heterogeneous electron donor—acceptor catalysis. *Nat. Commun.* **2023**, *14* (1), 7757.
- (26) Mo, K.; Yang, Y.; Cui, Y. A Homochiral Metal-Organic Framework as an Effective Asymmetric Catalyst for Cyanohydrin Synthesis. *J. Am. Chem. Soc.* **2014**, *136* (5), 1746–1749.
- (27) Xia, Q.; Li, Z.; Tan, C.; Liu, Y.; Gong, W.; Cui, Y. Multivariate Metal—Organic Frameworks as Multifunctional Heterogeneous Asymmetric Catalysts for Sequential Reactions. *J. Am. Chem. Soc.* **2017**, 139 (24), 8259–8266.
- (28) Ma, B.; Xia, Q.; Wang, D.; Jin, J.-K.; Li, Z.; Liang, Q.-J.; Sun, M.-Y.; Liu, D.; Liu, L.-J.; Shu, H.-X.; Yang, J.; Li, D.; He, J. Metal-Organic Framework Supported Copper Photoredox Catalysts for Iminyl Radical-Mediated Reactions. *Angew. Chem., Int. Ed.* **2023**, 62 (21), No. e202300233.
- (29) Ramirez, A.; Gevers, L.; Bavykina, A.; Ould-Chikh, S.; Gascon, J. Metal Organic Framework-Derived Iron Catalysts for the Direct Hydrogenation of CO₂ to Short Chain Olefins. *ACS Catal.* **2018**, 8 (10), 9174–9182.
- (30) Osadchii, D. Y.; Olivos-Suarez, A. I.; Szécsényi, Á.; Li, G.; Nasalevich, M. A.; Dugulan, I. A.; Crespo, P. S.; Hensen, E. J. M.; Veber, S. L.; Fedin, M. V.; Sankar, G.; Pidko, E. A.; Gascon, J. Isolated Fe Sites in Metal Organic Frameworks Catalyze the Direct Conversion of Methane to Methanol. *ACS Catal.* **2018**, 8 (6), 5542–5548.
- (31) Zheng, J.; Ye, J.; Ortuño, M. A.; Fulton, J. L.; Gutiérrez, O. Y.; Camaioni, D. M.; Motkuri, R. K.; Li, Z.; Webber, T. E.; Mehdi, B. L.; Browning, N. D.; Penn, R. L.; Farha, O. K.; Hupp, J. T.; Truhlar, D. G.; Cramer, C. J.; Lercher, J. A. Selective Methane Oxidation to Methanol on Cu-Oxo Dimers Stabilized by Zirconia Nodes of an NU-1000 Metal—Organic Framework. *J. Am. Chem. Soc.* **2019**, *141* (23), 9292—9304.
- (32) Grundner, S.; Markovits, M. A. C.; Li, G.; Tromp, M.; Pidko, E. A.; Hensen, E. J. M.; Jentys, A.; Sanchez-Sanchez, M.; Lercher, J. A. Single-site trinuclear copper oxygen clusters in mordenite for selective conversion of methane to methanol. *Nat. Commun.* **2015**, *6* (1), 7546.
- (33) Li, A.; Zhang, Y.; Sun, Z.; Niu, Z.; Lan, G. Photosensitizing metal-organic layers for photocatalysis, artificial photosynthesis and fluorescence imaging. *Sci. China Chem.* **2023**, *66* (12), 3372–3382.
- (34) Wang, H.; Zhang, C.; Dong, B.; Zhong, D.; Lu, T. Metalorganic layers: Preparation and applications. *Sci. China. Mater.* **2023**, 66 (3), 839–858.
- (35) Zhang, J.-H.; Yang, W.; Zhang, M.; Wang, H.-J.; Si, R.; Zhong, D.-C.; Lu, T.-B. Metal-organic layers as a platform for developing single-atom catalysts for photochemical CO₂ reduction. *Nano Energy* **2021**, *80*, No. 105542.
- (36) Wei, R.-J.; You, P.-Y.; Duan, H.; Xie, M.; Xia, R.-Q.; Chen, X.; Zhao, X.; Ning, G.-H.; Cooper, A. I.; Li, D. Ultrathin Metal—Organic Framework Nanosheets Exhibiting Exceptional Catalytic Activity. *J. Am. Chem. Soc.* **2022**, *144* (38), 17487–17495.

- (37) Cao, L.; Lin, Z.; Peng, F.; Wang, W.; Huang, R.; Wang, C.; Yan, J.; Liang, J.; Zhang, Z.; Zhang, T.; Long, L.; Sun, J.; Lin, W. Self-Supporting Metal—Organic Layers as Single-Site Solid Catalysts. *Angew. Chem., Int. Ed.* **2016**, *55* (16), 4962–4966.
- (38) Cao, L.; Wang, C. Metal-Organic Layers for Electrocatalysis and Photocatalysis. ACS Cent. Sci. 2020, 6 (12), 2149–2158.
- (39) Peng, X.; Pelz, P. M.; Zhang, Q.; Chen, P.; Cao, L.; Zhang, Y.; Liao, H.-G.; Zheng, H.; Wang, C.; Sun, S.-G.; Scott, M. C. Observation of formation and local structures of metal-organic layers via complementary electron microscopy techniques. *Nat. Commun.* **2022**, *13* (1), 5197.
- (40) Luo, T.; Fan, Y.; Mao, J.; Yuan, E.; You, E.; Xu, Z.; Lin, W. Dimensional Reduction Enhances Photodynamic Therapy of Metal—Organic Nanophotosensitizers. *J. Am. Chem. Soc.* **2022**, *144* (12), 5241–5246.
- (41) Feng, X.; Song, Y.; Lin, W. Dimensional Reduction of Lewis Acidic Metal—Organic Frameworks for Multicomponent Reactions. *J. Am. Chem. Soc.* **2021**, *143* (21), 8184–8192.
- (42) Fan, Y.; You, E.; Xu, Z.; Lin, W. A Substrate-Binding Metal—Organic Layer Selectively Catalyzes Photoredox Ene-Carbonyl Reductive Coupling Reactions. *J. Am. Chem. Soc.* **2021**, *143* (45), 18871–18876.
- (43) Fan, Y.; Zheng, H.; Labalme, S.; Lin, W. Molecular Engineering of Metal—Organic Layers for Sustainable Tandem and Synergistic Photocatalysis. *J. Am. Chem. Soc.* **2023**, *145* (7), 4158–4165.
- (44) Lan, G.; Fan, Y.; Shi, W.; You, E.; Veroneau, S. S.; Lin, W. Biomimetic active sites on monolayered metal—organic frameworks for artificial photosynthesis. *Nat. Catal.* **2022**, *5* (11), 1006–1018.
- (45) Lan, G.; Quan, Y.; Wang, M.; Nash, G. T.; You, E.; Song, Y.; Veroneau, S. S.; Jiang, X.; Lin, W. Metal—Organic Layers as Multifunctional Two-Dimensional Nanomaterials for Enhanced Photoredox Catalysis. *J. Am. Chem. Soc.* **2019**, *141* (40), 15767—15772.
- (46) Finkelstein, H. Darstellung organischer Jodide aus den entsprechenden Bromiden und Chloriden. Berichte der deutschen chemischen Gesellschaft 1910, 43 (2), 1528–1532.
- (47) Wang, J.-X.; Wang, Y.-T.; Zhang, H.; Fu, M.-C. Visible-light-induced iodine-anion-catalyzed decarboxylative/deaminative C–H alkylation of enamides. *Organic Chemistry Frontiers* **2021**, 8 (16), 4466–4472.
- (48) Fu, M.-C.; Shang, R.; Zhao, B.; Wang, B.; Fu, Y. Photocatalytic decarboxylative alkylations mediated by triphenylphosphine and sodium iodide. *Science* **2019**, *363* (6434), 1429–1434.
- (49) Ishiguro, K.; Nakano, T.; Shibata, H.; Sawaki, Y. Redox Reaction of Benzyl Radicals with Aromatic Radical Ions Photogenerated. The Marcus Inverted Region and the Selective Formation of Carbocations or Carbanions. *J. Am. Chem. Soc.* **1996**, *118* (31), 7255–7264.
- (50) Lowry, M. S.; Goldsmith, J. I.; Slinker, J. D.; Rohl, R.; Pascal, R. A.; Malliaras, G. G.; Bernhard, S. Single-Layer Electroluminescent Devices and Photoinduced Hydrogen Production from an Ionic Iridium(III) Complex. *Chem. Mater.* **2005**, *17* (23), 5712–5719.